ICAS-88-6.3.3 UNSTEADY SUPERSONIC FLOW COMPUTATIONS FOR ARBITRARY THREE-DIMENSIONAL CONFIGURATIONS

D. D. Liu*
Arizona State University
Tempe, AZ 85287

P. C. Chen†
Zona Technology, Inc.
Mesa, AZ 85202

and

Pablo Garcia-Fogeda**
Lab Aerodinamica
E.T.S.I. Aeronauticos
28040 - Madrid, Spain

ABSTRACT

Recent development of two unsteady supersonic methods for wing-body configurations are presented. These methods are the surface panel method (SPM) and the bundled triplet method (BTM). Both are based on the Harmonic Gradient Model. Extensive comparisons of computed results obtained from these two methods show good correlations with existing data. Cases compared range from the NACA and the NASA wing-body configurations to the NLR/F-5 wing with external stores to cylindrical flutter and to the Lockheed generic fighter (LGF). A two-model study of the LGF shows the insufficiency of the lifting surface model for a complete aircraft representation, which warrants a realistic wing-body model for accurate predictions of stability derivatives and flutter.

A computer program has been developed to integrate the use of the SPM and the BTM efficiently so that a complete aircraft with external stores can be treated effectively. For supersonic aeroelastic analyses, the computer program gives results that are accurate and cost effective, thus rendering it very favorable for industry applications.

INTRODUCTION

After over four decades of supersonic flight, it appears that few satisfactory methods exist for accurate predictions of supersonic unsteady airloads for realistic wing-body configurations. For computations of wing-body interference aerodynamics, the Doublet Lattice method[1,2] has been sufficiently developed to account for subsonic aeroelastic applications. By contrast, the development of its supersonic counterpart is restricted to the wing-alone[3-10] or the body-alone[11-13] configurations thus far.

Despite the importance of supersonic wing-body aerodynamics, only limited development can be found in the past. Earlier analytical work of Ward and Nielson[14,15] for steady flow and of Miles, Adam-Sears and Ashley, et al.[16-18] for unsteady flow have laid theoretical foundations in this area. Computational methods for the wing-body combinations for the steady linear subsonic/supersonic aerodynamics has been adequately developed by Woodward (USSAERO[19]) and the Boeing group (PANAIR[20]). For unsteady flow computations, a low-order panel method for wing-body combinations has been previously formulated by Morino et al.;[21] however, the paper did not provide sufficient validation to prove the method's applicability.

Apart from the aeroelastic problems on the airframe iteself, the problem of the wing-external store interaction is of no less importance. During the maneuver phase of a fighter aircraft, the latter type of interaction will change the unsteady airload and can also alter the flutter characteristics of the wing-tail drastically. In particular, problems such as underwing pylon/store and tip missile/wing interference are among the more critical problems in aircraft flutter. Although some progress has been made in this area,[22,23] the methods employed are not adequate to handle the supersonic aeroelastic problems.

In this paper, we present our recent development of two supersonic panel methods for unsteady treatments of arbitrary wing-body configurations including external-store systems. Both methods are based on our developed Harmonic Gradient model (HGM) for lifting surfaces[9] and for elastic bodies[11-13]. The first method uses the surface source panels for body representation and doublet panels for lifting surface representation. This method is termed the surface panel method (SPM),[24] which can be considered as the unsteady generalization of the USSAERO method, with the exception of the wing thickness effect. The second method uses a bundle of lines with low-order singularity to replace the SPM for handling sufficiently slender bodies. This method is termed the Bundled Triplet Method (BTM)[25] because lines of combined sources and doublets are employed to account for the generalized asymmetric bodies. The merit of BTM is that it renders no numerical leakage on the body surface and hence the solutions obtained asymptote to the slender body limit. Due to the nature of surface panel formulation, the SPM could not yield the slender body limit but it has the advantage of ease of applications to arbitrary wing-body configurations. At any rate, both methods are completely general in terms of the input wing-body geometry, mode shape and reduced frequency. Hence, they could complement each other effectively for aerodynamic and flutter calculations for a complete aircraft including external stores.

In what follows, extensive comparison of our computed results show good correlation with existing data which validate these methods. Cases of comparison range from asymmetric bodies to NLR/F-5 wing with external stores and to Lockheed generic fighters.

WING-BODY FORMULATION

The perturbed supersonic potential for a wing-body can be expressed as

$$\phi = \int_{A_B}\int \sigma H \, d\xi \, d\eta + \int_{A_W}\int \lambda \frac{\partial H}{\partial n} \, d\xi \, d\eta \qquad (1)$$

where σ and λ are the surface source strength and the surface doublet strength on the body surface, A_B and the wing surface A_W, respectively. The Kernel function here is defined as

* Associate Professor
† President
** Assistant Professor

$$H = e^{-i\mu M\xi} \cos \mu\bar{R}/\bar{R} \qquad (2)$$

where $\mu = kM/\beta$, k is the reduced frequency, M is the freestream Mach number, $\bar{R}$ is the hyperbolic distance between the singularity point x and the field point x_0 and $\xi \equiv x_0 - x$.

On the wing-body surface, the unsteady source and doublet strengths can be determined according to the tangency condition,

$$\begin{bmatrix} \left(\frac{\partial\phi}{\partial n}\right)_{BB} & \left(\frac{\partial\phi}{\partial n}\right)_{BW} \\ \left(\frac{\partial\phi}{\partial n}\right)_{WB} & \left(\frac{\partial\phi}{\partial n}\right)_{WW} \end{bmatrix} \begin{Bmatrix} \sigma \\ \lambda \end{Bmatrix} = \begin{Bmatrix} F_B \\ F_W \end{Bmatrix} \qquad (3)$$

where $F_W = h_{W_X} + i\,k\,h_W$ is the conventional thin wing downwash, and $F_B = F_B(n, u_0, h_B; k, M, \tau)$ is a complicated body downwash formula involving the mean flow velocity u_0, body thickness τ, etc.[11] The inverse of the square matrix on the LHS of Eq (3) is the Aerodynamic Influence Coefficient matrix, known as AIC.

The pressure coefficients for the body reads

$$C_{p_B} = C_{p_0} + \delta_0 (C_{p_1}) \cos\theta\, e^{ikt} \qquad (4a)$$

where

$$C_{p_0} = 2\left[S_0^{\gamma} - 1\right] / (\gamma M^2)$$

is the steady mean flow pressure coefficient and $C_{p_1} = -2S_0J_1$ is the unsteady flow pressure coefficient. Explicit expression of $S_0 = S_0(u; M, \gamma)$ and $J_1 = J_1(R, g, u_0, u_1, k)$ can be found in Ref. 12, where γ is the specific heat ratio. Decoupled from the mean flow, the unsteady pressure coefficient for thin wings is simply:

$$C_{p_w} = -2\left(\frac{\partial}{\partial x_0} + ik\right)\phi_1 e^{ikt} \qquad (4b)$$

HARMONIC GRADIENT METHOD

Space launch vehicles such as Saturn IB, where the body length is large, are required to scale up the reduced frequency range over 1.0. (See Refs. 12 and 13). The composite wings or tails of aircraft also have higher natural frequencies than those of the isotropic counterpart. To date, accurate aerodynamic prediction in the higher reduced frequency range is of particular concern for aeroelastic analysis.

To achieve computation accuracy and effectiveness in the high-reduced frequency and/or low Mach number domains, it is essential to render the source and the doublet solutions uniformly valid in the complete k and M domain. This can be simply achieved by modeling the source/doublet solutions to remain spatially harmonic in the mean flow direction. In so doing, the panel size $\Delta\xi_j$ is regulated and made compatible with the compressible reduced frequency μ. This is known as the Harmonic Gradient (H-G) Model established in Refs. 11, 12 and 13.

Application of the H-G model to Eq (1) amounts to stating that in the interval $\Delta\xi_j$

$$\sigma = a\left(1 - e^{-i\mu\xi}\right) \qquad (5a)$$

for the source panel and

$$\lambda = \left(b\,\xi + d\right) e^{-i\mu\xi} \qquad (5b)$$

for the doublet panel (see Figure 1).

Owing to this model, optimal number of panels can be achieved, and yet it is least affected by the given reduced frequency and the Mach number.

Since the first publication of the Harmonic Gradient Method (HGM) for lifting surfaces in 1983, the method has been further advanced to a version based on an acceleration potential formulation. In fact, it is this advanced version that provides the basis for the present wing-body scheme. Throughout the last five years, this advanced version of HGM has been improved several times, properly documented and made compatible with NASTRAN for flutter applications. To date, the improved version of the documented code of HGM is known as the ZONA51 code among the industrial users. However, in what follows, we shall refer to the whole improved work as HGM for simplicity.

BUNDLED TRIPLET METHOD

The surface panel method (SPM) described in the formulation has been fully developed for arbitrary wing-body configurations in Ref. 25 (see Fig. 2). This work can be considered as the generalization of Woodward's work (USSAERO[19]) into the unsteady domain.

However, during the course of this development we found that the SPM in general would not provide a correct numerical limit when the body thickness approaches that of a slender body, say $\tau \lesssim 5\%$. This would prevent us from accurate treatments of slender missiles or stores. Furthermore, when multiple underwing stores are considered, the total panel number for SPM would increase substantially. It is realized that some sort of line doublet method must be developed in parallel so that it will complement SPM for aerodynamic computations of aircraft with stores.

We have now developed a new method using a bundle of combined low-order singularities to replace the surface panel method for handling sufficiently slender bodies. This method is termed Bundled Triplet Method (BTM[24]). (It should be noted that the BTM is equally capable of handling both thick or slender bodies). To be exact, the low-order singularities used are lines of sources and doublets. The generalized triplet potential is thus defined as

$$\phi_m = \int a_m H d\xi + \left(\int b_m \frac{\partial H}{\partial r} d\xi\right)\cos\theta_m + \left(\int c_m \frac{\partial H}{\partial r} d\xi\right)\sin\theta_m \qquad (6)$$

where a_m is the line source strength, and b_m and c_m are the line doublet strengths in the sector $\theta_m < \theta < \theta_{m+1}$ (see Fig. 2). The discretized unknown strengths a_{im}, b_{im} and c_{im} are related to the triplet potential ϕ_{im} by a least square matrix. In so doing, ϕ_{im} can be solved through the tangency conditions.

When a_m and c_m are set to zero, BTM is reduced to the line doublet method (also known as the HPP method, (see Refs. 11 and 12 and Figs. 3 and 4) as a special case. Hence, BTM can effectively handle axisymmetric as well as asymmetric bodies of arbitrary shapes including slope discontinuities. When

in combined use with SPM, it is seen that BTM can be equally applicable to wing-body combinations (Fig. 5). In terms of computing time, BTM could be many times faster than the SPM; also, less panel number is required for BTM for the same body. In the case of a smoothed axisymmetric body, for example, only twenty panels are needed for HPP whereas five to ten times more panels are needed for SPM.

COMPUTED RESULTS

The results presented herein are selected from various sources from our computed data file. The legends used in the figures and for which the method is used therefore require clarification. The list below is provided to the reader for this purpose.

Method	Reference	Figures
HGM (ZONA51)	9	6, 7-11, 24
BTM	24	12, 14-18, 19
SPM	25	13, 20, 21, 22 23, 25

Nonplanar Canard/Wing Configuration

Figure 6 presents the lifting distributions for a canard/wing configuration at various span locations. Due to the low value of the given Mach number, M = 1.145891 (corresponding to Mach angle $\mu = 60°$), all edges are subsonic except the wing trailing edge. As can be seen in Fig. 6, good agreement is found in all spanwise stations between the present results and those obtained by USSAERO and both methods capture the subsonic (near sonic) trailing edge and supersonic trailing edge behavior for canard and wing, respectively.

Lockheed Generic Fighter

Figure 7 shows the Lockheed generic fighter (LGF) configuration together with its local and global coordinates. Figure 8 shows the panel arrangement for the LGF in which four subsystems are defined according to the ZONA51 code. A total of 228 panels are used to model this configuration. It is noted that the fuselage of LGF is being modeled by a lifting surface (Subsystem 1).

Figures 9a, 10a and 11a present the steady lifting pressure distributions ΔC_p at M = 1.2 as computed by HGM and USSAERO on the modeled fuselage, the canard, and the wing, and the fin, respectively. While all leading edges are subsonic, the canard has a nearly-sonic subsonic trailing edge, both the wing and the fin have supersonic trailing edges. Good agreement with USSAERO is found for all the spanwise sections considered and both methods confirm the proper edge behaviors.

Unsteady pressure distributions, real and imaginary ΔC_p's of all subsystems are shown in Figs. 9b, 10b and 11b. The complete aircraft is pitching about a pitching axis located at 51.65% of the fuselage length aft the apex at a reduced frequency of 1.0.

Asymmetric Bodies

The BTM is used to compute all cases in this category. In Figs. 12a and 12b, the steady pressure distributions are presented for two conical bodies with considerable asymmetry at Mach number M = 2.0 and at mean angle of attack $\alpha = 0°$.

Since the flowfields are conical and symmetrical about the meridian plane, only the circumferential C_p pressures on half of the body are presented ($0 \le \theta \le 180°$). Because of the steeper variation in the given body curvature of Fig. 12b, a bundle of 36 triplet lines is distributed in equal circumferential intervals for a full body. The body geometry in Fig. 12a has relatively smooth curvature variations; hence, only 18 triplet lines are used to account for a full body. It can be seen that the present computed result is in good agreement with Devan's results using a finite difference method[26] and the USSAERO results.[19] Typically, we use 40 panels in the circumferential direction in the USSAERO program. In the x-direction, 5 equally spaced segments are used for both the USSAERO and the BTM Codes. For the latter this amounts to a total of 100 to 200 panels and equal numbers of control points to be evaluated. Because the evaluation scheme of the present kernel is much simpler, the CPU time required is about one tenth of that needed in the USSAERO code.

Elliptic Cones

Fig. 13 presented below is computed using SPM whereas Figs. 14 through 18 are computed by BTM. Fig. 13 presents pressure distribution of an elliptic cone ($\sigma = 6°$) at steady mean angles of attack, $\alpha_0 = 0°$, 3° and 6°. The present computed results are compared with those of USTORE code,[27] USSAERO code,[19] and the measured data.[28] It should be noted that the present method practically recovers the results of USSAERO code. This is expected since the present method is based on the surface-panel method (SPM) which contains the USSAERO formulation as a special case for k = 0. A parallel checking on the same case has been conducted using the line-doublet method (HPP method[12]). Our preliminary finding indicates that the present SPM is superior to HPP method when ellipticity ratio, a/b is below 1/3.

In Figs. 14, 15 and 16, a series of studies on the effects of ellipticity ratio, a/b (defined as the minor axis to major axis ratio), on the static and dynamic stability derivatives are presented for a family of elliptic cones. The pitching axis is placed at the cone apex and a freestream Mach number M = 3.0 is given for all cases. Both C_{N_α} and C_{M_α} decrease with increasing ellipticity. Good agreement is found in Figs. 14 and 15 between the present results and those of USSAERO. This trend is expected since reducing the ellipticity ratio implies the elliptic cone is further collapsed into a low-aspect-ratio delta wing configuration. The damping-in-pitch normal force and moment coefficient versus ellipticity ratio are shown in Fig. 16. whereas no available data are found for comparison. When the pitching axis is placed at apex, the present results indicate that a delta wing-like body (a < b) tends to be more unstable than a circular cone (a = b) statically as well as dynamically.

In Figs. 17 and 18, the in-phase and the out-of-phase pressure coefficients for the same elliptic cone family in first-mode bending oscillations at a reduced frequency k = 1.0 are shown. In Fig. 17, the unsteady pressures are plotted along the x-axis in the meridian plane ($\theta = 0$) whereas in Fig. 18, along the azimuthal angle θ at the base section (x = 1). When the ellipticity ratio approaches one, all results check with those obtained by the HPP method for a right circular cone.[13] While the dependency on ellipticity ratio is relatively insensitive for the pressures along the x-axis, strong dependency is shown along the azimuthal direction.

Cylindrical Panel Flutter

In order to validate the BTM method in the high-frequency domain, supersonic cylindrical flutter cases (Fig. 19) are selected for comparison with existing theories (Refs. 29 and 30).

A bundle of triplet lines are arranged according to a cosine distribution both in the circumferential ($0 \le \theta \le 2\pi$) and in the axial directions ($0 \le x \le 1$). The cylindrical panel is first evenly divided into n intervals in the circumferential direction, say n = 5. Within each interval, eight control points are used,

given a total of 40 control points. In the axial direction, 25 points are used for all n's. The real and imaginary part of the generalized forces on the cylindrical panel are presented in Figs. 9b and 9c for the freestream Mach number $M_\infty = \sqrt{2}$ and the reduced frequencies k = 0 and 1.0.

It is seen that good agreement is found between the present results in terms of generalized forces Q_{11} and those of Dowell and Widnall[29] and of Platzer et al.[30] up to n = 5 for both reduced frequencies.

Steady Wing-Body Interference

Longitudinal loadings (C_n d/d_{max}) over a 10% thick body of revolution with and without a tapered wing (AR = 4.0 and Tapered Ratio = 0.6) are presented in Fig. 20.

The force coefficient C_n is defined as

$$C_n = \frac{1}{d} \int_0^{2\pi} C_p \, d\theta$$

where d and d_{max} represent the diameter and maximum diameter of the body, respectively.

No interference effect is noted in the first 40% of the body length, as expected. A bump-like loading along 40% to 85% body length is observed as a result of the presence of the tapered wing. In addition, lifting pressure distribution along the wing chord is also plotted at the 20% semi-spanwise location. Good agreement is found in the present computed results with those measured in Ref 31. Thus, the steady aerodynamic option of the Surface Panel method is validated by means of this present interference example.

NACA Wing-Body

Fig. 21b presents the computed lift curve slopes, C_{L_α}, for the body only, wing only and the wing-body cases. It is seen that the wing only case (a delta wing as shown in Fig. 21a) produces the highest lift slope as expected, whereas, in contrast, the body only case produces relatively insignificant lift slope throughout the Mach number range considered. Notice that the present C_{L_α} value is based on the wing surface area. Typical C_{L_α} for bodies uses the based area. A conversion formula reads:

$$(C_{L_\alpha})_{present} = \left(\frac{\text{Wing Area}}{\text{Body Base Area}} \right) (C_{L_\alpha})_{body}$$

The present wing-body result tends to underpredict the C_{L_α} slightly. However, the damping-in-pitch moments at the pitching axis location 0.35 c and 0.45 c, as shown in Figs. 21c and 21d, indicate slight overprediction of our wing-body results, while the wing-only results are in better agreement with the measured data.

It should be noted that the slight overprediction of the damping moments by the present method in comparison with the measured data could be subject to a number of factors. These include the aeroelastic effect of the wind tunnel model as well as the induced viscous effects as pointed out previously in Ref. 32.

Other computed cases of delta-wing body, unswept- and swept- wing body combinations are also found in good agreement with the measured data. These comparisons can be found in Refs. 24 and 25, in which the computations were performed using SPM and BTM respectively.

NLR Underwing Store

In Fig. 22a, a NLR wind-tunnel test configuration constructed with a F-5 wing plus an underwing store is modeled by 112 body panels representing the missile body, 72 wing panels the F-5 wing, 6 panels the pylon, 10 panels the launcher, and 24 panels the four aft fins. The complete configuration is in pitching oscillation about 50% root chord at a circular frequency ω = 20 Hertz and at freestream Mach number M = 1.35.

Figure 22b shows the computed in-phase and the out-of-phase unsteady pressure distributions (one-half of the real ΔC_p and imaginary ΔC_p, respectively) in three spanwise locations for a clean wing and for the same wing with an underwing-store. The NLR measured data for the latter are also presented here for comparison.[33] In the outboard spanwise location, up to 10% difference in the computed ΔC_p's appear to be unsmoothed, which could be caused by the uncertainties occurring in the test. The computed imaginary ΔC_p's in general show a close trend to that obtained by the measurement.

In Fig. 22c, the integrated spanwise unsteady normal forces and pitching moments along the F-5 wing under the influence of the complete underwing store system are plotted against those of the clean wing case according to the computed results and the test data.

The unsteady force and moment coefficients in this figure are defined as:

The sectional normal force:

$$C_{z\,i} = \frac{1}{\pi} \int_0^1 \Delta C_p \, d\,(x/c)$$

The sectional pitching moment:

$$C_{m\,i} = \frac{2}{\pi} \int_0^1 \Delta C_p \, (x/c - 0.25) \, d\,(x/c)$$

where c is the local chord length.

It is seen that the computed forces and moments predict the same trend as the measured data showing a finite discontinuity across the pylon location. The computed results tend to overestimate the in-phase forces and moments and underestimate the out-of-phase forces and moments in comparison with the measured data.

However, these discrepancies may be caused by the uncertainties in the measured unsteady data as mentioned in Ref. 33. Meanwhile NLR also provided the measured quasi-steady data, which is supposedly more reliable for the in-phase forces. Better agreement in trend between the quasi-steady data and the computed results is found for this case.

NLR Wing-with-Tip Missile

In Fig. 23a another NLR wind-tunnel test configuration constructed with F-5 wing with tip missile is modeled by 72 wing panels for the F-5 wing, 14 panels for the pylon, 16 panels for the four canard fins, 24 panels for the four aft fins, and 112 body panels for the missile body. This configuration was tested under the same conditions as those provided for the NLR Underwing Store cases.

Similar to Fig. 22b, the computed results of unsteady pressure distributions ΔC_p's are plotted, for a clean wing and for the same wing with tip-missiles, against three spanwise locations. It is seen that at the outboard location (97.1%), the real ΔC_p for the wing with tip-missile exceeds twice that of the clean wing value. As expected the tip-missile influence on the wing pressure gradually lessens as the spanwise location approaches to 18.1% The measured real ΔC_p's in the present case also appear to be unsmoothed. However, the present results predict the same trend as that obtained by

measurement.[33] Overall, the local influence of the tip-missile on the wing pressure is substantial as compared with that of the underwing store on the wing.

The unsteady spanwise normal forms and pitching moments for a clean F-5 wing and the complete Wing-with-tip Missile are plotted along the semispan in Fig. 23c.

The results obtained for the clean wing and the Wing-with-tip Missile cases depart from each other at 60% semi-span toward the wing tip. This is expected since the influence domain of the tip missile to the wing is bounded by the forward Mach cone emanating from the missile apex.

Similar to Fig. 22c, the computed results in the present case tend to overpredict the in-phase forces and moments and underpredict the out-of-phase forces and moments in comparison with the measured data. Again, these discrepancies may be caused by the uncertainties in the measurement as mentioned in Ref. 33. Better agreement in trends can be observed between the more reliable NLR quasi-steady data and the present results.

Wing Flutter Study

Flutter characteristics of a swept delta (swept angle Λ = 70°) mounted on a body of revolution has been studied by NASA Langley Research Center using the HGM method (ZONA51 Code). As shown in Figs. 24a and 24b, the body is assumed to be rigid and flexible for cases A and B, respectively. Seven modes on the wing are assumed for case A, whereas three free-free modes on the body and four modes on the wing are assumed for case B. All wing modes are selected from the dominant flutter modes used by Hanson and Levey.[34]

Cases at four Mach numbers (M = .8, 1.2, 2.5, 3.0) are computed as shown in Figs. 24c and 24d for the rigid body and the flexible body cases, respectively. Three supersonic codes are used for computations; these are indicated by PISTON (piston theory, e.g., Ref. 35), ACUNN (Atlee Cunningham, Refs. 3 and 4) and ZONA (actually ZONA51/HGM, Ref. 9). In Fig. 24c, it is seen that ZONA compared well with those of PISTON at two higher Mach numbers 2.5 and 3.0 and with ACUNN at M = 1.2, while ACUNN over- and underestimates these values at the higher Mach numbers. On the other hand, the test results by Hanson and Levey shown from M = .8 to 1.2 are obtained under a different condition where the wing under consideration is mounted on a flat wing tunnel wall. The verification of the test data therefore awaits further generation of computed results.

Flutter points obtained by three codes agree well in Fig. 24d for the flexible body case. Note that ZONA generated consistently the most conservative boundary. All codes predict a jump in the flutter boundaries at M = 2.5. Presumably, it is caused by the mechanism of flutter-mode switching at this Mach number.

Several simplifications are noted for these calculations. First, all dynamic pressures of flutter Q (in psi) are computed based on a fixed speed of sound, namely a = 1000 ft/sec. Second, the wing-body effects are included only structurally but not aerodynamically in these studies, since the three codes used are confined to treatments of lifting surfaces only.

Wing-Body Model of LGF

Here, the case of the Lockheed Generic Fighter (LGF) is revisited. In constrast to the lifting-surface model (Model A) presented earlier, a realistic wing-body model (Model B) has been presently developed according to the SPM in Ref. 24. In Fig. 25, Model A is basically the same configuration shown in Figs. 7 and 8; Model B is constructed by replacing the lifting-surface "fuselage" with an elliptic cone-cylinder body of equivalent width and one-quarter of the width as its height.

In Tables 1a, 1b and 1c, the stability derivatives are computed for three Mach numbers (M = 1.2, 1.35 and 1.5) for the configurations performing rigid pitching oscillations. A breakdown on each of the configuration components is also included. The stability derivatives therein are defined as follows:

$$C_{L_\alpha} = \frac{Re(Q_{12})}{S}$$

$$C_{M_\alpha} = \frac{Re(Q_{22})}{S\bar{c}}$$

$$C_{L_{\dot\alpha}} + C_{L_q} = \frac{Im(Q_{12})}{S k}$$

$$C_{M_{\dot\alpha}} + C_{M_q} = \frac{Im(Q_{22})}{S\bar{c} k}$$

where S is the reference area S = 187.

$\bar{c}$ is the mean aerodynamic chord $\bar{c}$ = 10.377

$k = \frac{W\bar{c}}{U_\infty}$ is the reduced frequency,

k is taken as 0.05 in the present analysis.

$Q_{12, 22}$ are the 12 and 22 components of the computed 2 x 2 generalized forces matrix with two rigid body modes. The first mode is the plunging mode and the second is the pitching mode about the pitching axis located at $\frac{X_r}{\bar{c}}$ = 1.67668.

Several observations can be made from the obtained stability derivatives. First, at M = 1.5 (Table 1c) C_{L_α} of Model B $(C_{L_\alpha})_B$ = 3.029, compares well with the test value $(C_{L_\alpha})_{test}$ = 3.048. The lifting surface model yields a value of $(C_{L_\alpha})_A$ = 3.376, indicating more than 10% lift is generated excessively due to an inappropriate modeling of the fuselage. Second, longer damping moment is obtained for Model B at a lower Mach number (M = 1.2) whereas it levels off to a slightly lower value than those of Model A at M = 1.35 and 1.5. In particular, the damping moments for the fin show a loss of damping at M = 1.2 for Model B, but a negative damping value for Model A, i.e. $(C_{M_{\dot\alpha}} + C_{M_q})_A$ = - .379. Apparently, the lifting surface model totally fails to predict such an instability of the fin.

These observations indicate that a realistic model such as Model B is mandatory for accurate prediction of unsteady forces and moments. It is expected that the lifting surface model would be unsatisfactory for this purpose as well as for that of flutter predictions.

CONCLUSION

Two methods for unsteady supersonic computations of wing-body configurations are presented. It is suggested that the surface panel method (SPM) and the bundled triplet method (BTM) should be in combined use for effective predictions of unsteady aerodynamics for complex aircraft configurations. Extensive comparison of our computed results show good correlation with existing data which validate our methods. Comparison examples include asymmetric bodies, NACA Wing-body NLR/F-5 wing with external stores and Lockheed Generic Fighter (LGF) configurations.

Two-model study of the LGF shows the insufficiency of the lifting surface model for aircraft which warrants a realistic wing-body representation for accurate flutter predictions.

In view of the present development, we believe that an integrated three-dimensional unsteady supersonic method for arbitrary wing-body configurations is finally at hand. It is apparent that the present method could pair with the Doublet Lattice method to perform unified supersonic/subsonic analyses for realistic aircraft.

A production computer code has also been developed whose capabilities include: handling arbitrary configurations

with multiple external stores, aircraft components defined in subsystems, line/surface spline logics, full frequency range input, automated paneling scheme, etc. The program is designed to handle a wide range of aeroelastic computations. With these features, the program provides an accurate and effective tool for supersonic aeroelastic analyses which suggest immediate industrial applications.

REFERENCES

1. Rodden, W.P., Giesing, J.P. and Kalman, T.P., "New Developments and Applications of the Subsonic Doublet Lattice Method for Nonplanar Configurations," AGARD Symposium on Unsteady Aerodynamics for Aeroelastic Analyses of Interfering Surfaces, Paper No. 4, May 1970.

2. Giesing, J.P. and Kalman, T.P., "Oscillatory Supersonic Lifting Surface Theory Using a Finite Element Doublet Representation," AIAA Paper 75-761, 1975.

3. Cunningham, A.M., Jr., "Oscillatory Supersonic Kernel Function Method for Interfering Surface," Journal of Aircraft, Vol. 11, No. 11, 1974, pp. 664-670.

4. Cunningham, A.M., Jr., "Oscillatory Supersonic Kernel Function Method for Isolated Wings," Journal of Aircraft, Vol. 11, No. 10, 1974, pp. 609-615.

5. Jones, W.P. and K. Appa, "Unsteady Supersonic Aerodynamics Theory for Interfering Surfaces by the Method of Potential Gradient," NASA CR-2898, 1977.

6. Hounjet, M.H.L., "An Improved Potential Gradient Method to Calculate Airloads on Oscillating Supersonic Interfering Surfaces," Journal of Aircraft, Vol. 19, No. 15, 1982.

7. Ueda, T. and Dowell, E.H., "Doublet-Point Method for Supersonic Unsteady Lifting Surfaces," AIAA Journal, Vol. 22, No. 2, February 1984, pp. 179-186.

8. Lottati, I. and Nissim, E., "Nonplanar Supersonic Three-Dimensional Oscillatory Piecewise Continuous Kernel-Function Method," Journal of Aircraft, Vol. 24, No. 1, January 1987.

9. Chen, P.C. and Liu, D.D., "A Harmonic Gradient Method for Unsteady Supersonic Flow Calculations," Journal of Aircraft, Vol. 22, No. 5, May 1985, pp. 371-379.

10. Appa, K., "Constant Pressure Panel Method for Supersonic Unsteady Airload Analysis," Journal of Aircraft, Vol. 24, No. 10, Oct. 1987, pp. 696-702.

11. Garcia-Fogeda, P. and Liu, D.D., "A Harmonic Potential Panel Method for Flexible Bodies in Unsteady Supersonic Flow," AIAA Paper No. 86-007, 1986; also Vol. 24, No. 12, Journal of Aircraft, Dec. 1987, pp. 833-840.

12. Garcia-Fogeda, P. and Liu, D.D., "Aeroelastic Applications of Harmonic Potential Panel Method to Oscillating Flexible Bodies in Supersonic Flow," AIAA Paper No. 86-0864-CP, 1986.

13. Liu, D.D., Garcia-Fogeda, P. and Chen, P.C., "Oscillating Wings and Bodies with Flexure in Supersonic Flow - Application of Harmonic Potential Panel Method," ICAS Paper 86-2.9.4, 1986; also to appear in Journal of Aircraft.

14. Wards, G.N., *Linearized Theory of Steady High-Speed Flow,* Part III Slender Body Theory, Cambridge at the University Press, 1955.

15. Nielsen, J.N., "Quasi-cylindrical Theory of Wing-Body Interference at Supersonic Speeds and Comparison with Experiment," NACA Report 1252, 1955.

16. Miles, J.W., *The Potential Theory of Unsteady Supersonic Flow*, Cambridge University Press, 1959.

17. Adams, M.C. and Sears, W.R., "Slender-Body Theory - Review and Extension," Journal of the Aeronautical Sciences, Vol. 20, No. 2, 1953, pp. 85-98.

18. Zartarian, G. and Ashley, H., "Forces and Moments on Oscillating Slender Wing-Body Combinations at Supersonic Speed - I. Basic Theory," OSR TN No. 57-386, 1957.

19. Woodward, F.A., "Analysis and Design of Wing-Body Combinations at Subsonic and Supersonic Speeds," Journal of Aircraft, Vol. 5, No. 6, Nov.-Dec. 1968, pp. 528-534.

20. Tinoco, E.N., Johnson, F.T. and Freeman, L.M., "Application of a Higher Order Panel Method to Realistic Supersonic Configurations," Journal of Aircraft, Vol. 17, No. 1, January 1980.

21. Morino, L., Chen, L.T. and Suciu, E.O., "Steady and Oscillating Subsonic and Supersonic Aerodynamics Around Complex Configuration," AIAA Journal, Vol. 13, March 1975.

22. Sotomayer, W.A., Dusto, A.R., Epton, M.A. and Johnson, F.T., "Aerodynamic Modeling of Oscillating Wing with External Stores," AIAA Paper 81-0648, May 1981.

23. Roos, R., Bennekers, B. and Zwann, R.J., "A Calculation Method for Unsteady Subsonic Flow about Harmonically Oscillating Wing-Body Configuration," AIAA Paper 75-854.

24. Garcia-Fogeda, P., Chen, P.C. and Liu, D.D., "Unsteady Supersonic Flow Calculations for Wing Body Combinations Using Harmonic Gradient Method," AIAA Paper 88-0568.

25. Chen, P.C. and Liu, D.D., "Unsteady Supersonic Computations of Arbitrary Wing-Body Configurations Including External Stores," AIAA Paper 88-2309-CP.

26. Devan, L., "Conical, Noncircular, Second-Order Potential Theory of Supersonic Flow," AIAA Journal, Vol. 22, May 1984, pp. 618-623.

27. Van der Broek, G.J., "The Analytical Prediction of the Separation Behavior of External Stores after Release from the Carrier Aircraft, Part II - Applications," NIAST 79/103, August 1979.

28. Maslen, S.H., "Pressure Distribution on Thin Conical Body of Elliptic Cross-Section at Mach Number 1.89," NACA RM E8K05, 1949.

29. Dowell, E.H. and Widnall, S.E., "Generalized Aerodynamic Forces on an Oscillating Cylindrical Shell," Quarterly of Applied Mathematics, No. 1, 1966, pp. 1-17.

30. Platzer, M.F., Brix Jr., C.W. and Webster, K.A., "Linearized Characteristics Method for Supersonic Flow Past Vibrating Shells," AIAA Journal, Vol. 11, No. 9, 1973, pp. 1302-1305.

31. Loving, D.L. and Estabrooks, B.B., "Transonic-Wing Investigation in the Langley 8-Foot High-Speed Tunnel at

High Subsonic Mach Numbers and at a Mach Number of 1.2," NACA RM L51F07, September 1951.

32. Tobak, M., "Damping-in-Pitch of Low Aspect-Ratio Wings at Subsonic and Supersonic Speeds," NACA RM A52L04a, 1953.

33. Tijdeman, J., et al., "Transonic Wind Tunnel Tests on an Oscillating Wing with External Stores; Part I-IV, The Wing with Tip Store," Air Force Flight Dynamics Laboratory, Wright Patterson Air Force Base, OH, AFFDL-TR-78-194, May 1979.

34. Hanson, P.W. and Levey, G.M., "Experimental and Calculated Results of a Flutter Investigation of Some Very Low Aspect-Ratio Flat-Plate Surfaces at Mach Numbers from 0.62 to 3.00," NASA TN D-2038, October, 1963.

35. Ashley, H. and Zartarian, G., "Piston Theory - A New Aerodynamic Tool for the Aeroelastician," J. of the Aeronautical Sciences, Vol. 23, No. 12, December 1956, pp. 1109-1118.

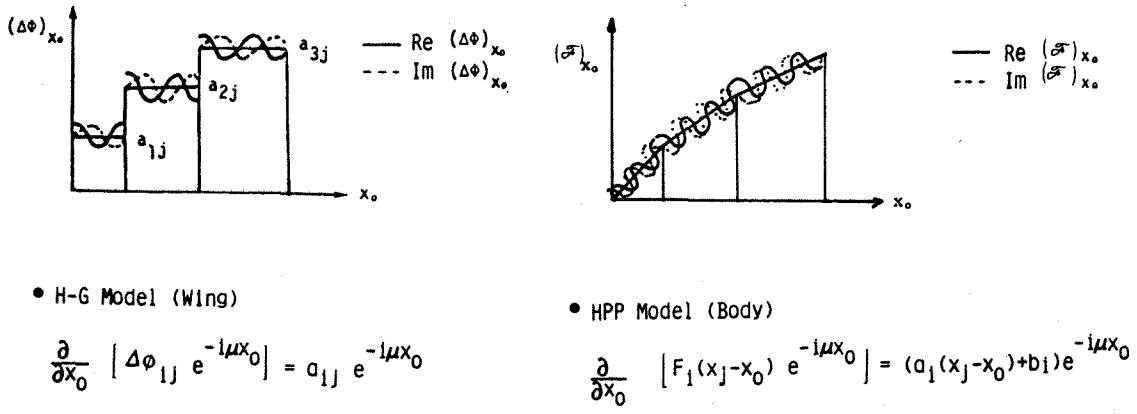

Fig. 1 Harmonic Gradient Model for Wings and Bodies.

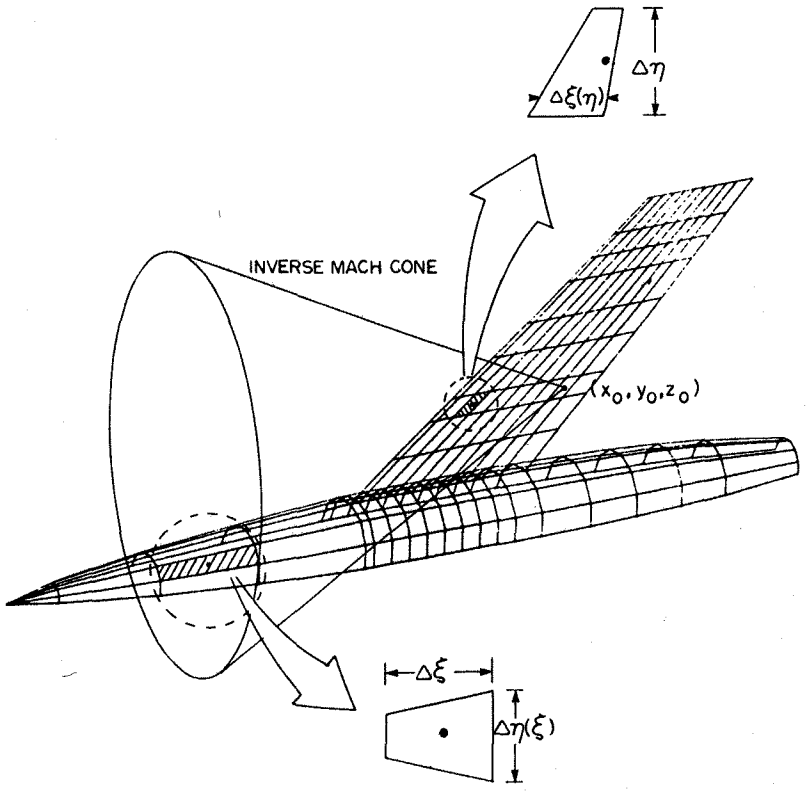

Fig. 2 Wing-Body Paneling Scheme.

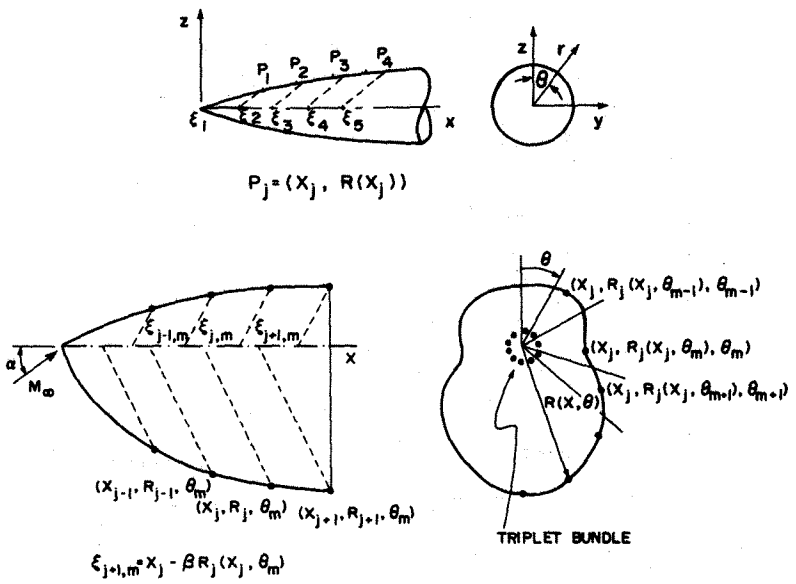

Fig. 3 Distributions of Line Doublets (HPP) and Bundled Triplets (BTM).

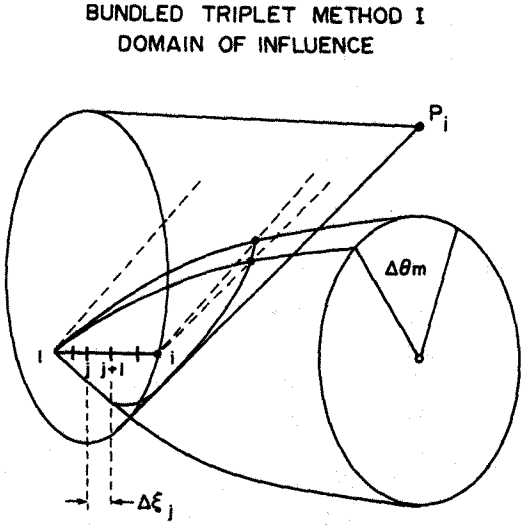

Fig. 4 Bundled Triplet Method (BTM): Domain of Influence.

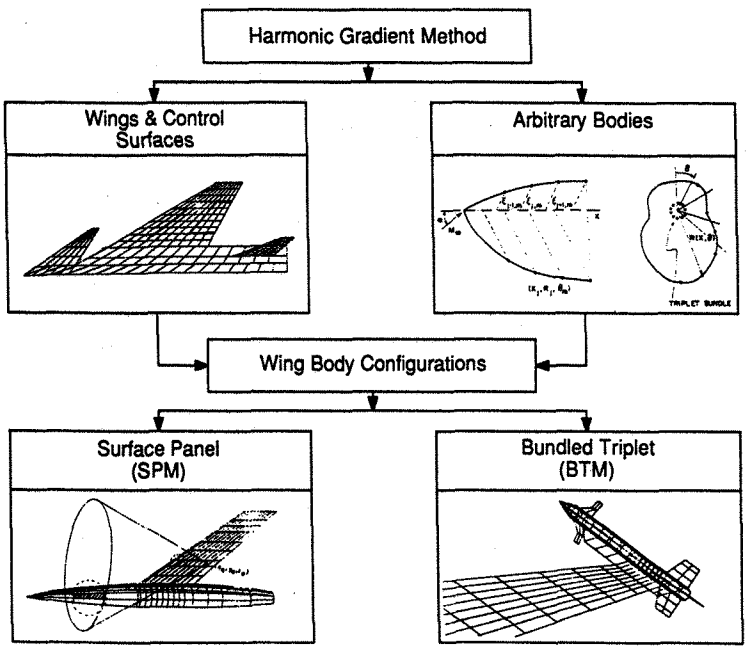

Fig. 5 Diagram Showing Unsteady Supersonic Development for Wing-Body Combinations.

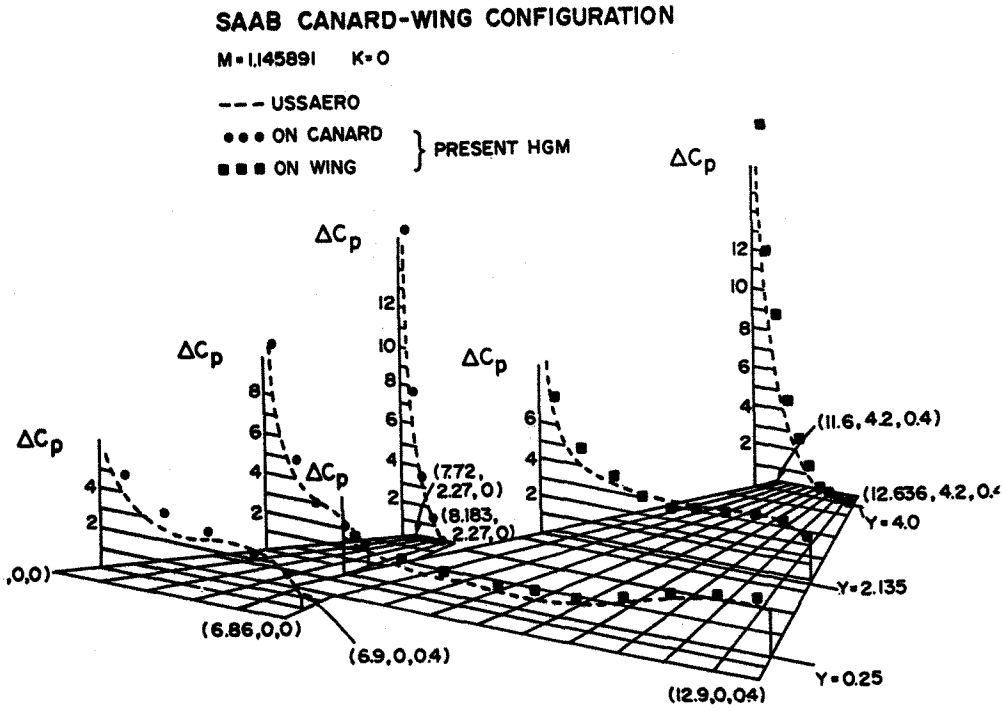

Fig. 6 Pressure Distribution on the Saab Canard-Wing Configuration.

LOCAL COORDINATES
(Zero Dihedral)

	X Fuselage Sta.	Y Buttline
	Fuselage-Wing	
A1	0.0	0.0
B1	3.8	1.05
C1	9.328	1.05
D1	13.183	3.1
E1	25.983	10.49
F1	28.779	10.49
G1	24.7	3.1
H1	33.686	3.1
I1	33.686	0.0
	Canard	
A2	0.0	0.0
B2	7.992	5.344
C2	8.815	5.344
D2	5.226	0.0
	Fin	
A3	0.0	0.0
B3	5.838	6.413
C3	7.188	6.413
D3	4.734	0.0

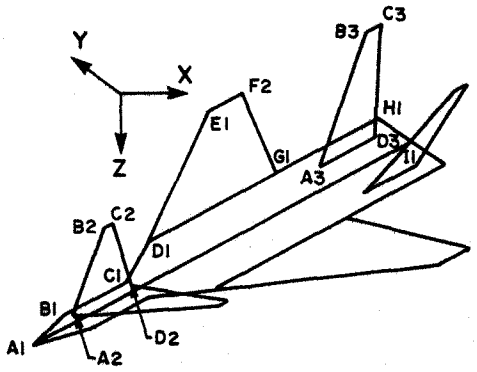

GLOBAL COORDINATES OF ORIGINS OF LOCAL AXES AND SURFACE ATTITUDES

	X	Y	Z	Dihedral	Incidence
Fuselage-Wing	0.0	0.0	-0.14	0.0 Deg	0.0 Deg
Canard	3.508	0.0	0.56	0.0	0.0
Fin	27.394	1.926	-0.14	70.5	0.0

Fig. 7 Lockheed Generic Fighter Configuration.

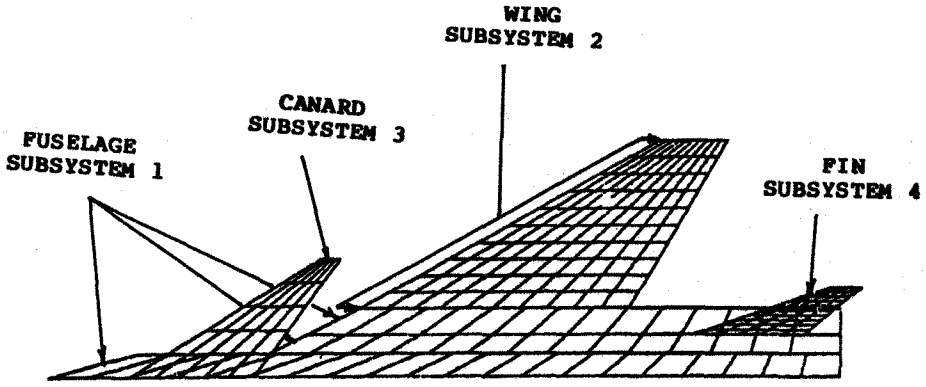

Fig. 8 Panel Arrangement for the LGF Configuration.

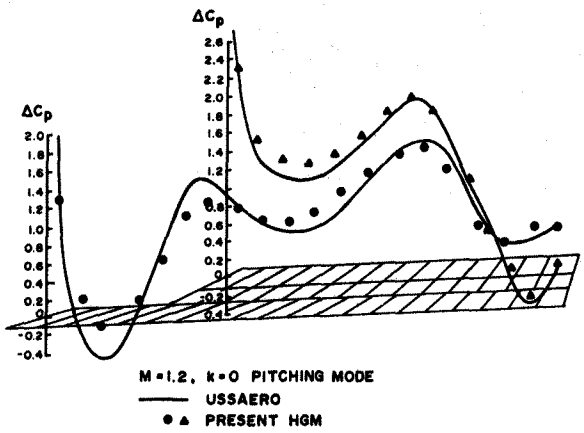

Fig. 9a Lifting Pressure Distribution on Modeled Fuselage at M = 1.2 and k = 0.

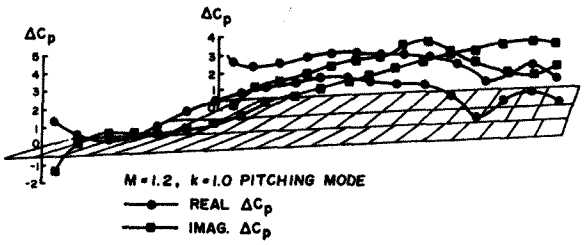

Fig. 9b Unsteady Pressure Distribution on Modeled Fuselage at M = 1.2 and k = 1.0.

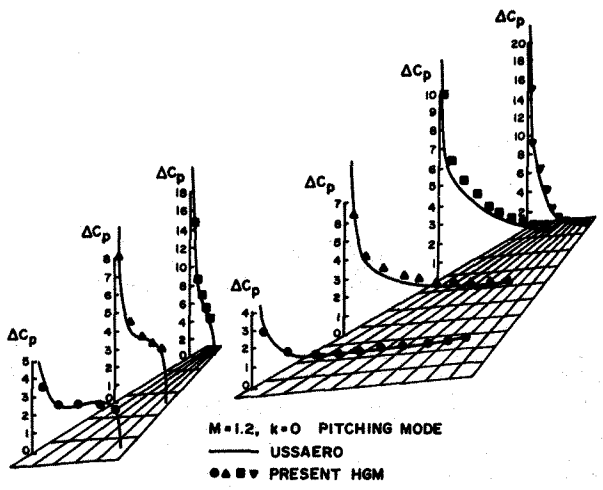

Fig. 10a Lifting Pressure Distribution on Canard and Wing at M = 1.2 and k = 0.

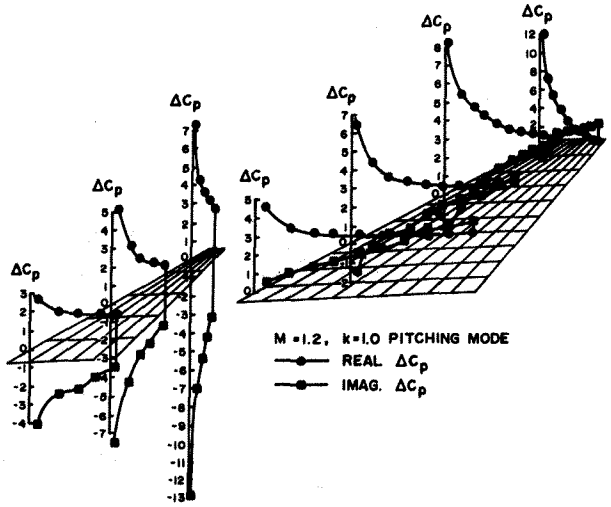

Fig. 10b Unsteady Pressure Distribution on Canard and Wing at M = 1.2 and k = 1.0.

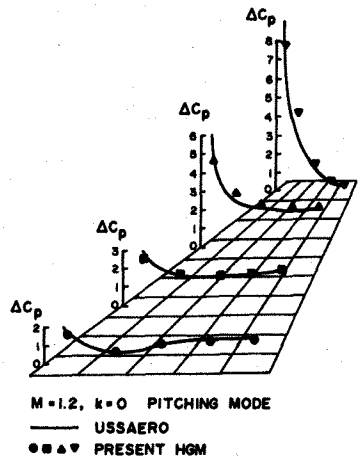

Fig. 11a Lifting Pressure Distribution on Fin at M = 1.2 and k = 0.

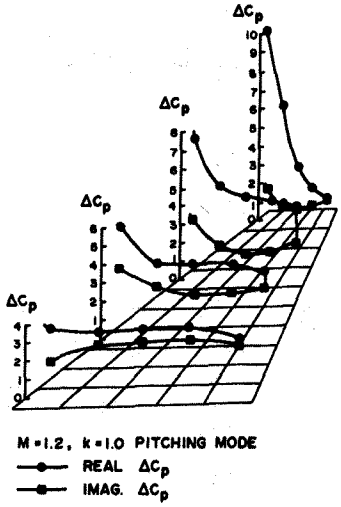

Fig. 11b Unsteady Pressure Distribution on Fin at M = 1.2 and k = 1.0.

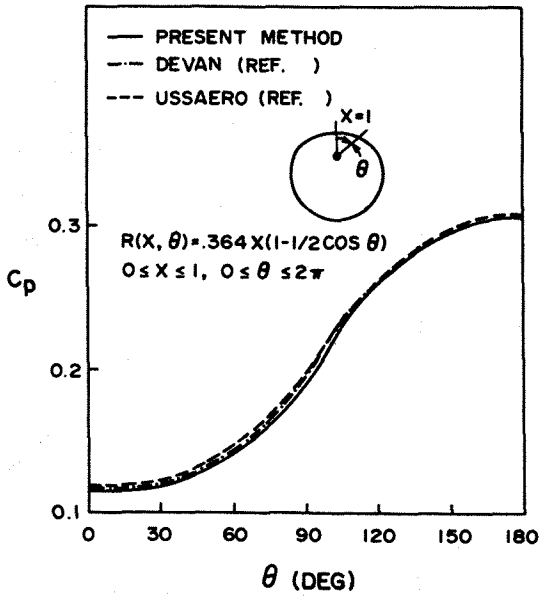

Fig. 12a Steady-mean Pressure Coefficient for an Asymmetric Cone at M = 2.0, α = 0°.

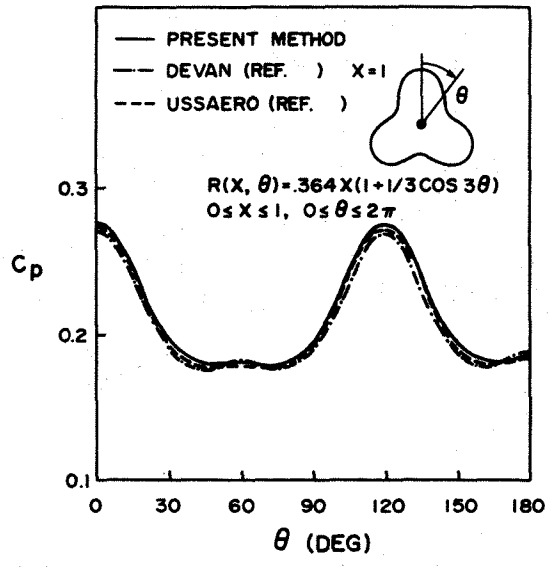

Fig. 12b Steady-mean Pressure Coefficient for an Asymmetric Cone at M = 2.0, α = 0°.

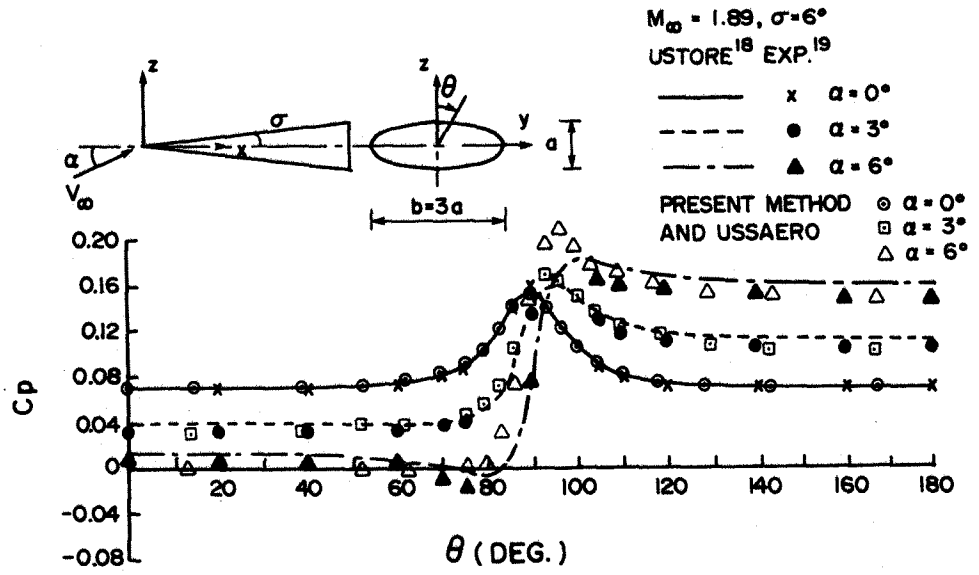

Fig. 13 Circumferential Steady Pressure Distributions on an Elliptic Cone at Various Angles of Attack.

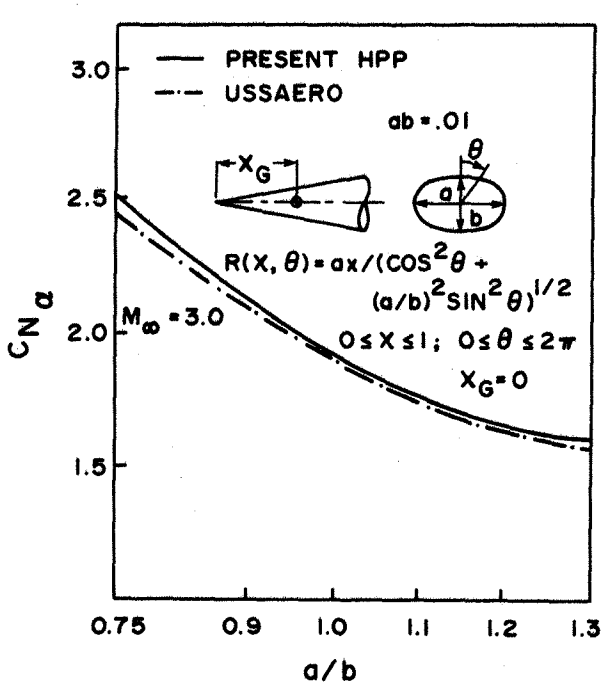

Fig. 14 Normal-force Coefficient for Elliptic Cones versus the Ellipticity Ratio a/b at M = 3.0.

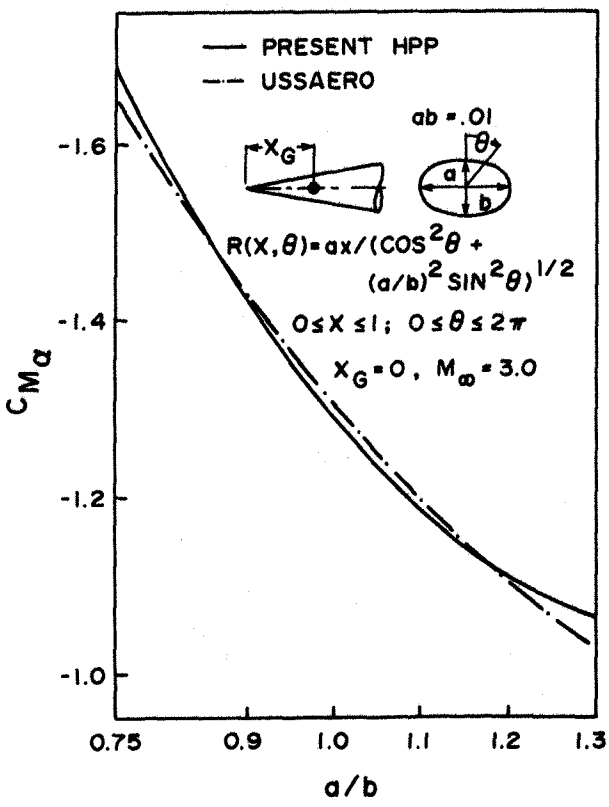

Fig. 15 Pitching Moment Coefficient for Elliptic Cones versus the Ellipticity Ratio a/b at M = 3.0.

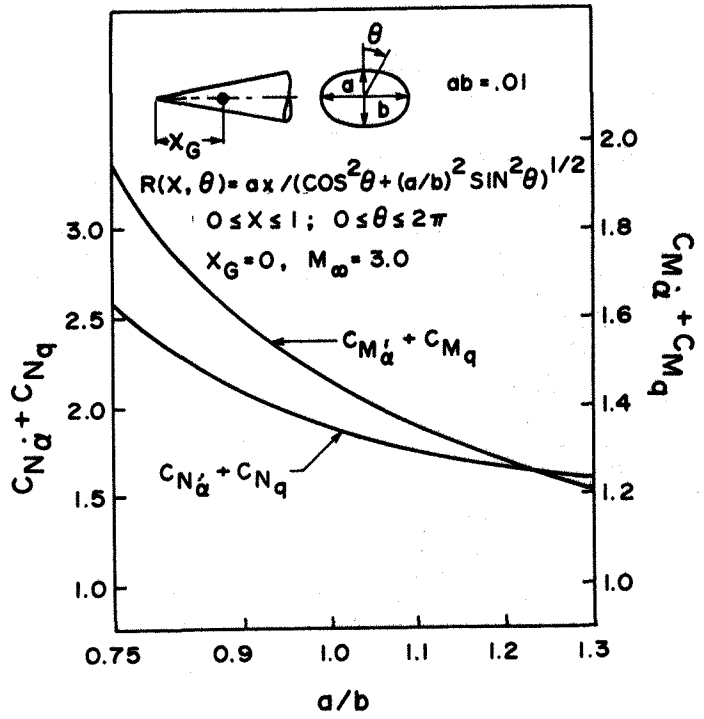

Fig. 16 Damping-in-pitch Normal-force Coefficient and Damping-in-pitch Moment Coefficient for Elliptic Cones versus the Ellipticity Ratio a/b at M = 3.0.

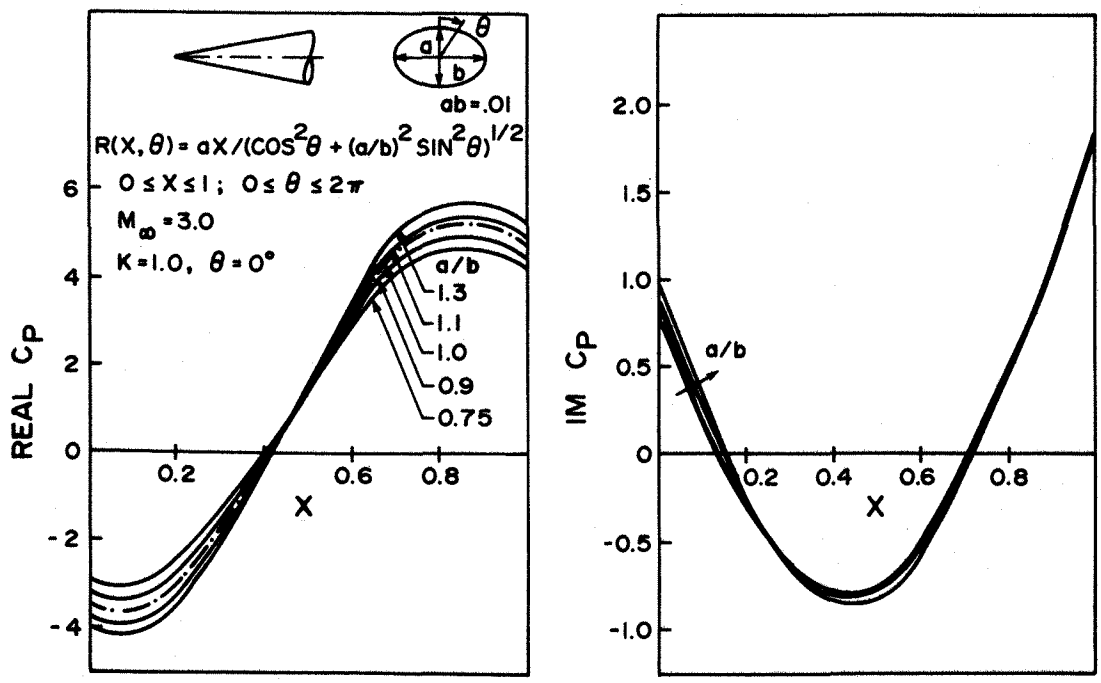

Fig. 17 In-phase and Out-of-phase Pressure Coefficient for Elliptic Cones in First Bending Mode at M = 3.0 and Reduced Frequency k = 1.0 along the X-axis.

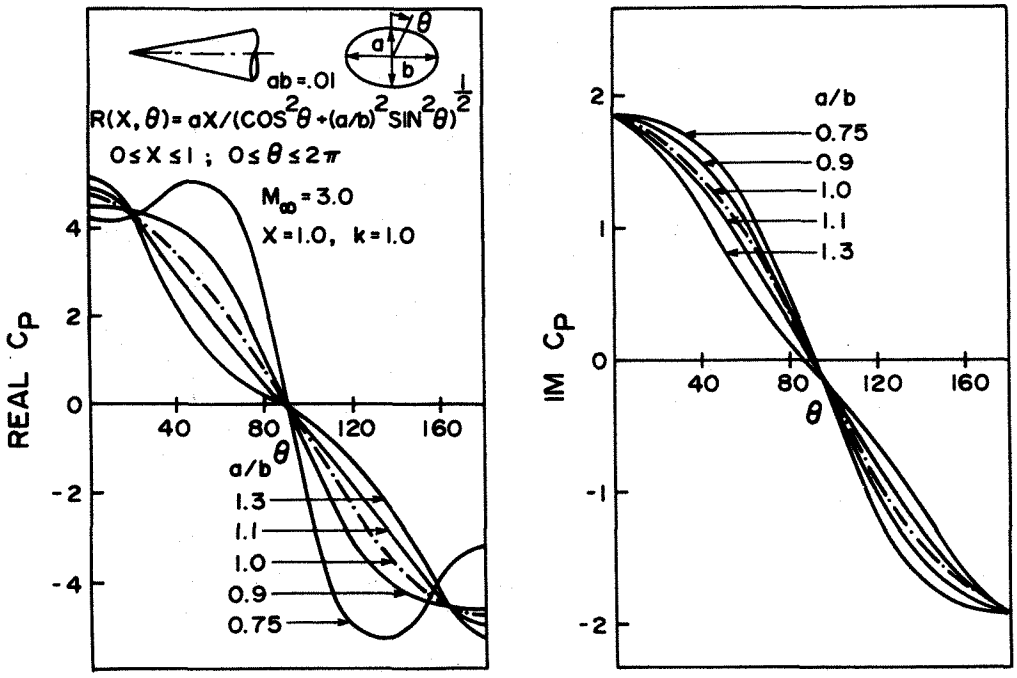

Fig. 18 In-phase and Out-of-phase Pressure Coefficient for Elliptic Cones in First Bending Mode at M = 3.0 and Reduced Frequency k = 1.0 along the Polar Angle.

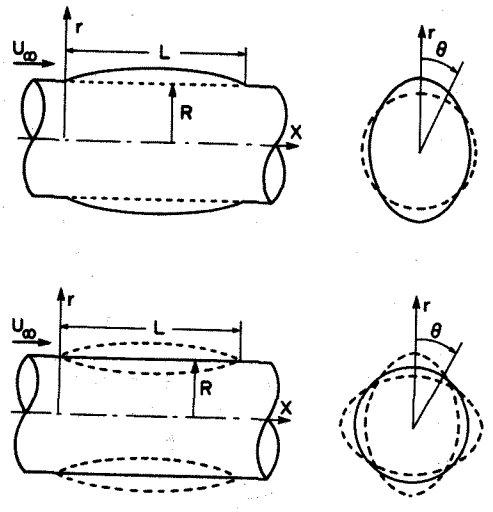

Fig. 19a Cylindrical Flutter Showing Two Vibrating Modes.

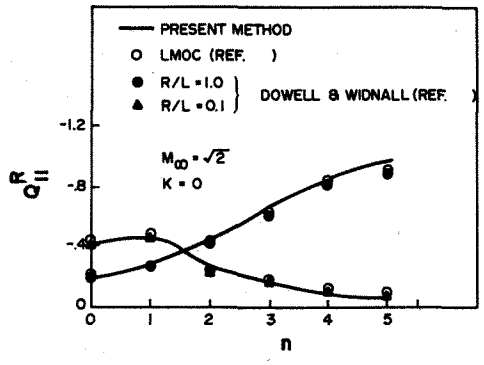

Fig. 19b Real Part of the Generalized Aerodynamic Force Q_{11} Versus Circumferential Mode Number.

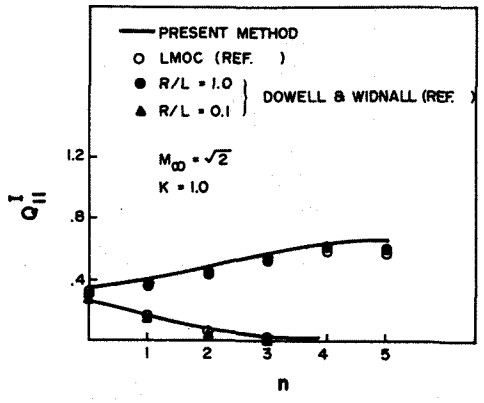

Fig. 19c Imaginary Part of the Generalized Aerodynamic Force Q_{11} Versus Circumferential Mode Number.

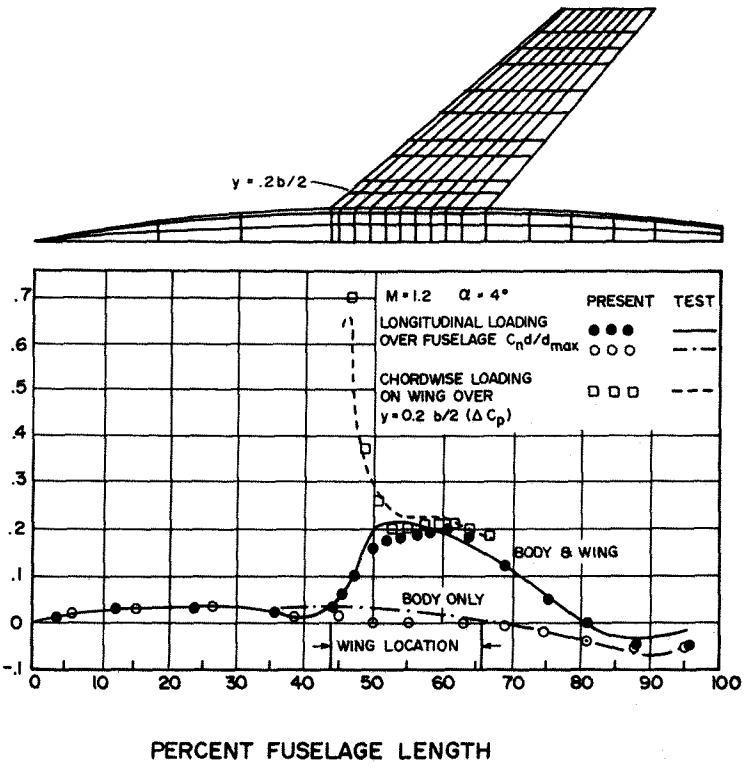

Fig. 20 Static Loadings About the Fuselage-Wing Junctions.

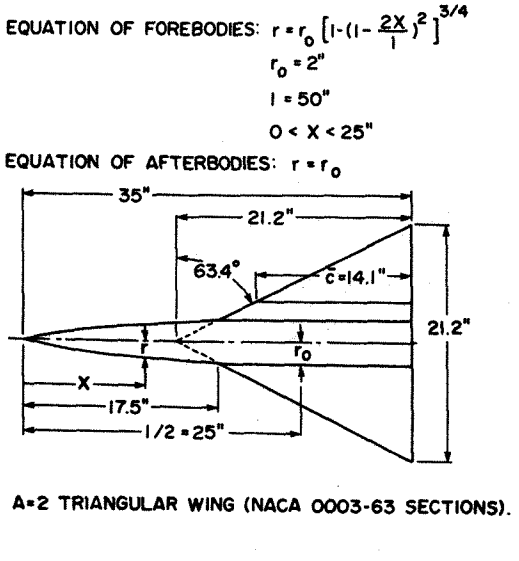

A=2 TRIANGULAR WING (NACA 0003-63 SECTIONS).

Fig. 21a Sketch of a Wing-Body Combination: Aspect Ratio AR = 2.0 Delta Wing with Centered Body of Revolution.

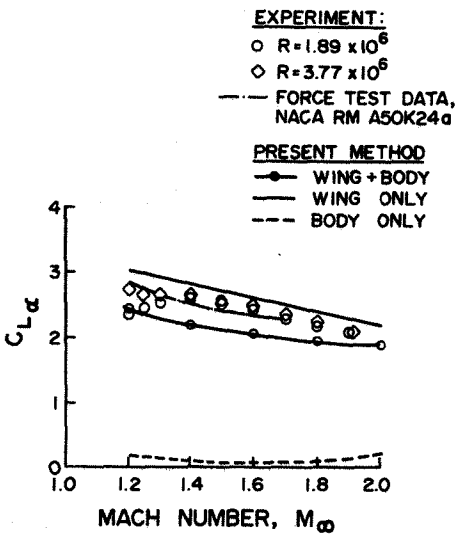

Fig. 21b Lift-Curve Slopes for a AR = 2.0 Wing-Body Combination.

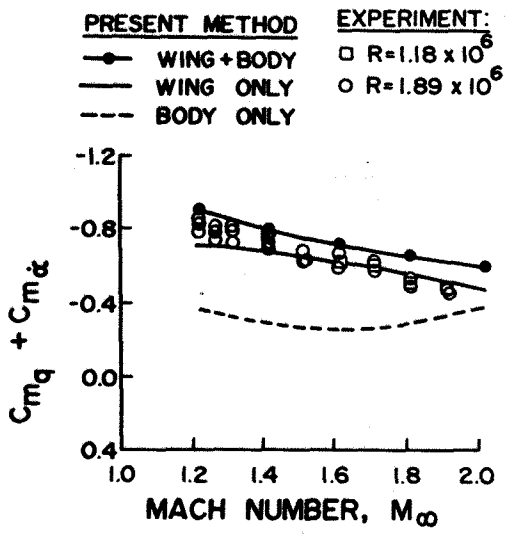

Fig. 21c Damping-in-pitch Moment Coefficients for an AR = 2.0 Wing-Body Combinations about Pitching Axis at 0.35c.

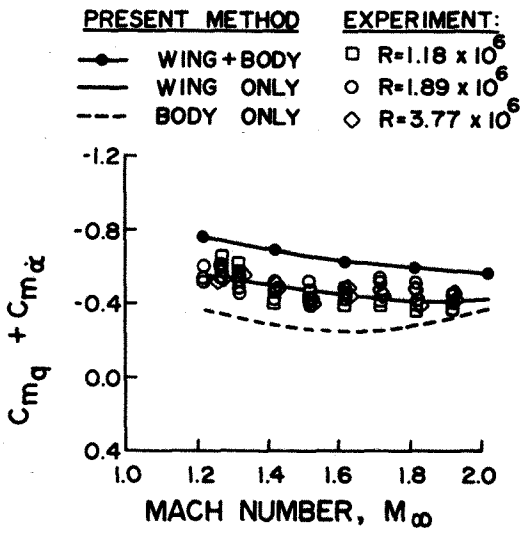

Fig. 21d Damping-in-pitch Moment Coefficients for an AR = 2.0 Wing-Body Combinations about Pitching Axis at 0.45c.

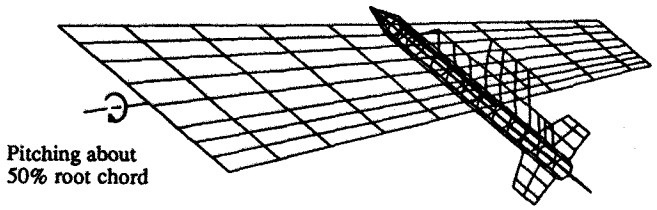

Fig. 22a Paneling Model for the Under-Wing Store Configuration: Northrop F-5 Wing plus Under-Wing Pylon, Launcher, Missile Body with Fore and Aft Fins.

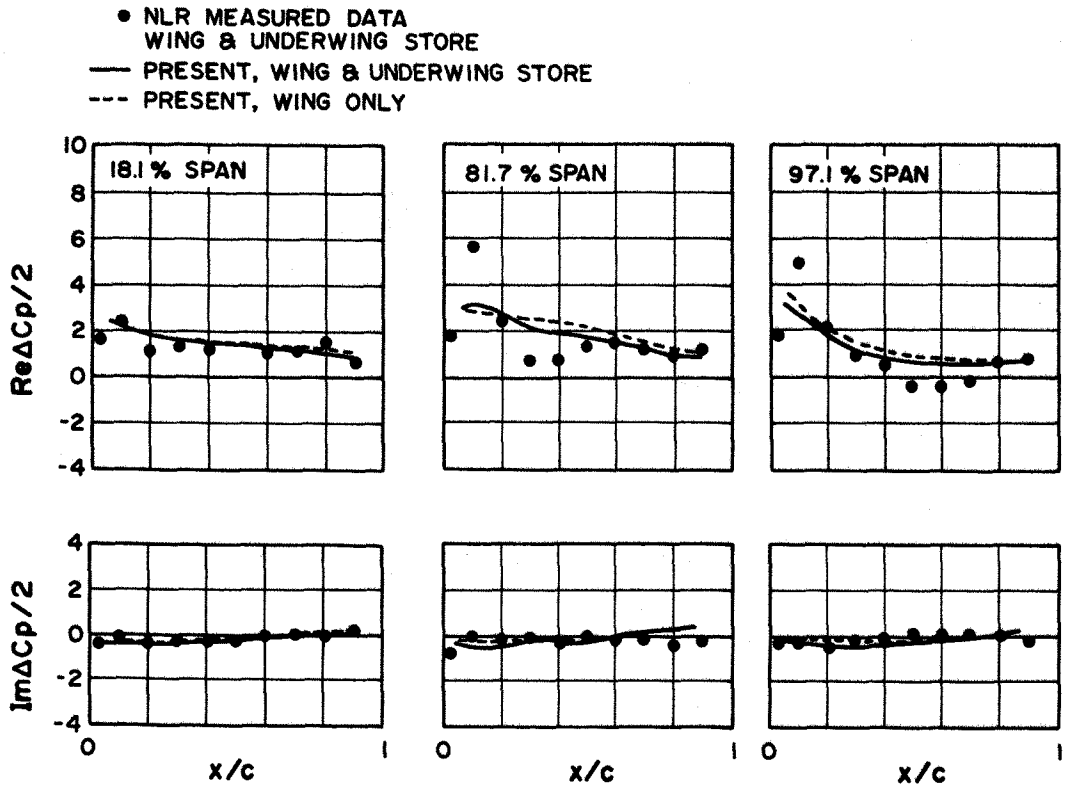

Fig. 22b Unsteady Pressure Distributions of the Clean F-5 Wing and the Under-Wing Store Configuration at $M_\infty = 1.35$ and Reduced Frequency $k = 0.1$.

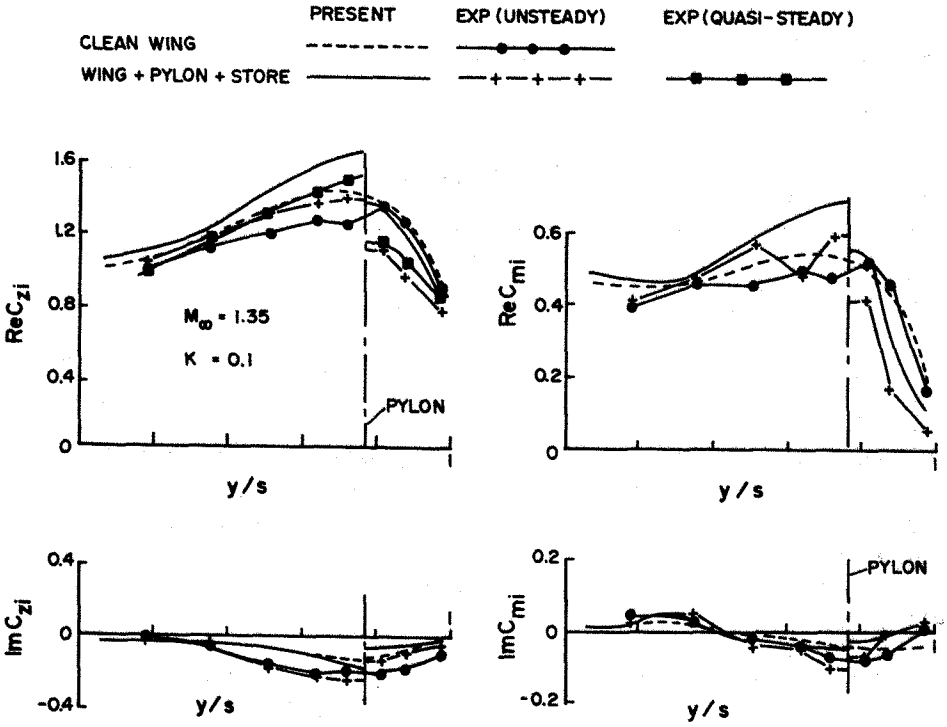

Fig. 22c Unsteady Spanwise Normal Force and Pitching Moment for the Clean F-5 Wing and the Under-Wing Store Configuration at $M_\infty = 1.35$ and Reduced Frequency $k = 0.1$.

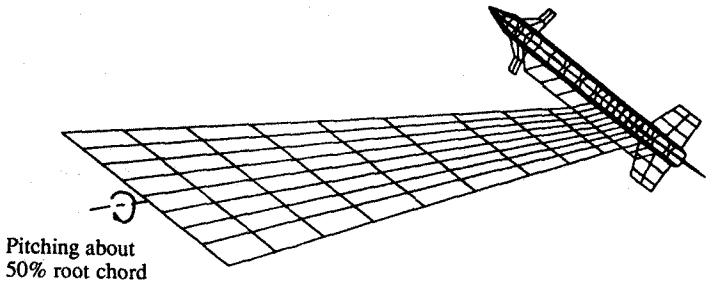

Fig. 23a Paneling Model for the Wing with the Tip Missile Configuration: Northrop F-5 Wing plus Launcher, Missile Body with Fore and Aft Fins.

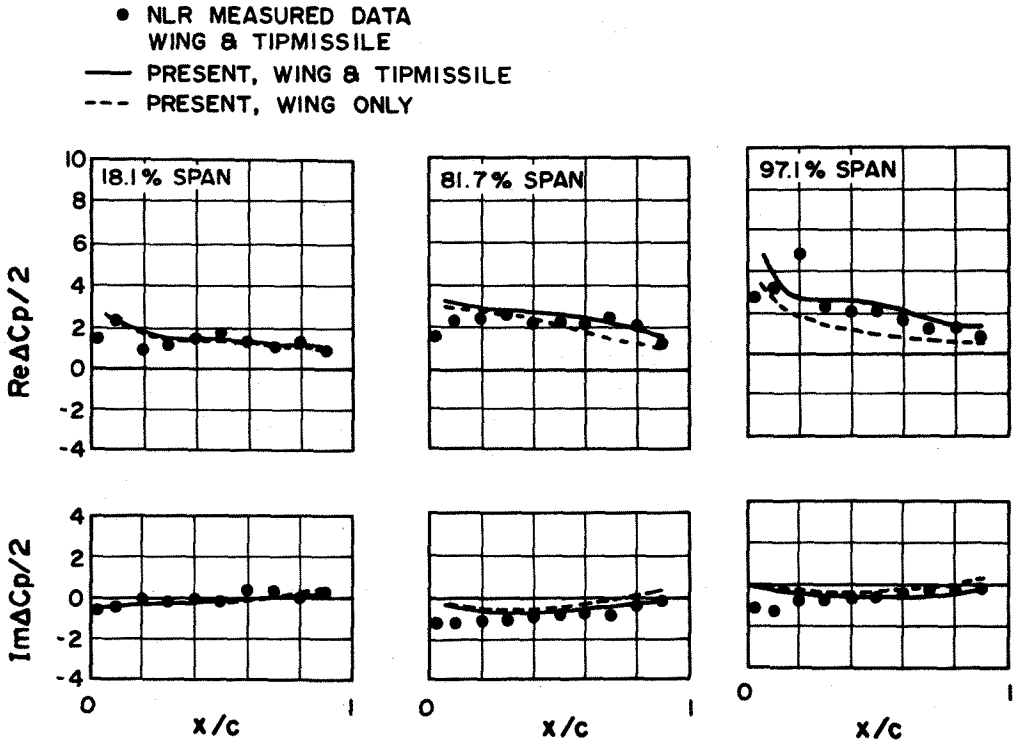

Fig. 23b Unsteady Pressure Distributions of the Clean F-5 Wing and the Complete Wing-with-Tip Missile Configuration at $M_\infty = 1.35$ and Reduced Frequency $k = 0.1$.

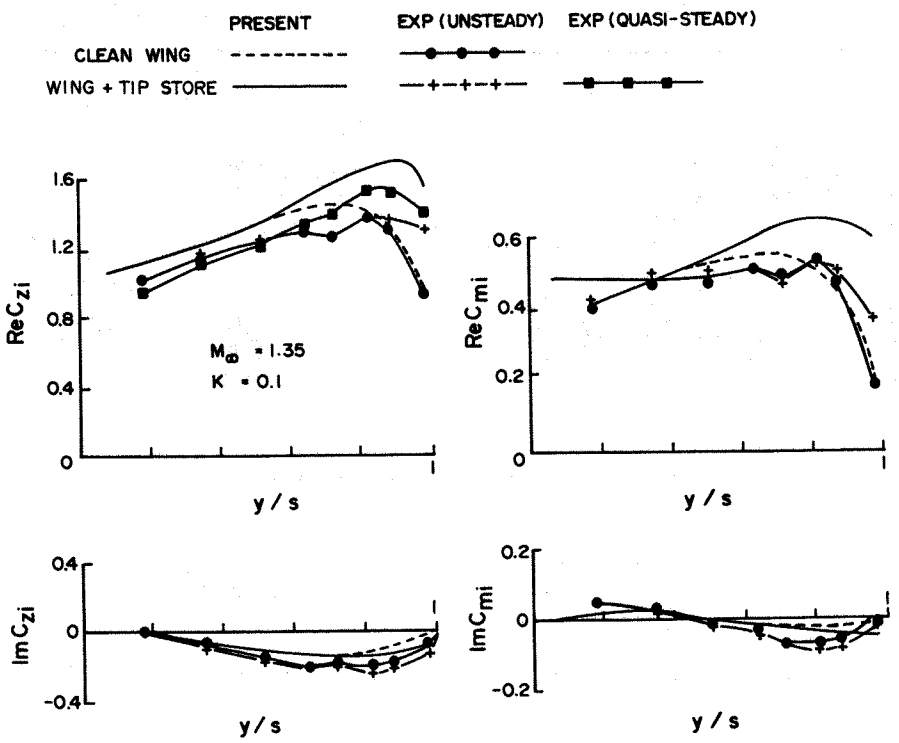

Fig. 23c Unsteady Spanwise Normal Forces and Pitching Moment for the Clean F-5 Wing and the Complete Wing-with-Tip Missile Configuration at $M_\infty = 1.35$ and Reduced Frequency k = 0.1.

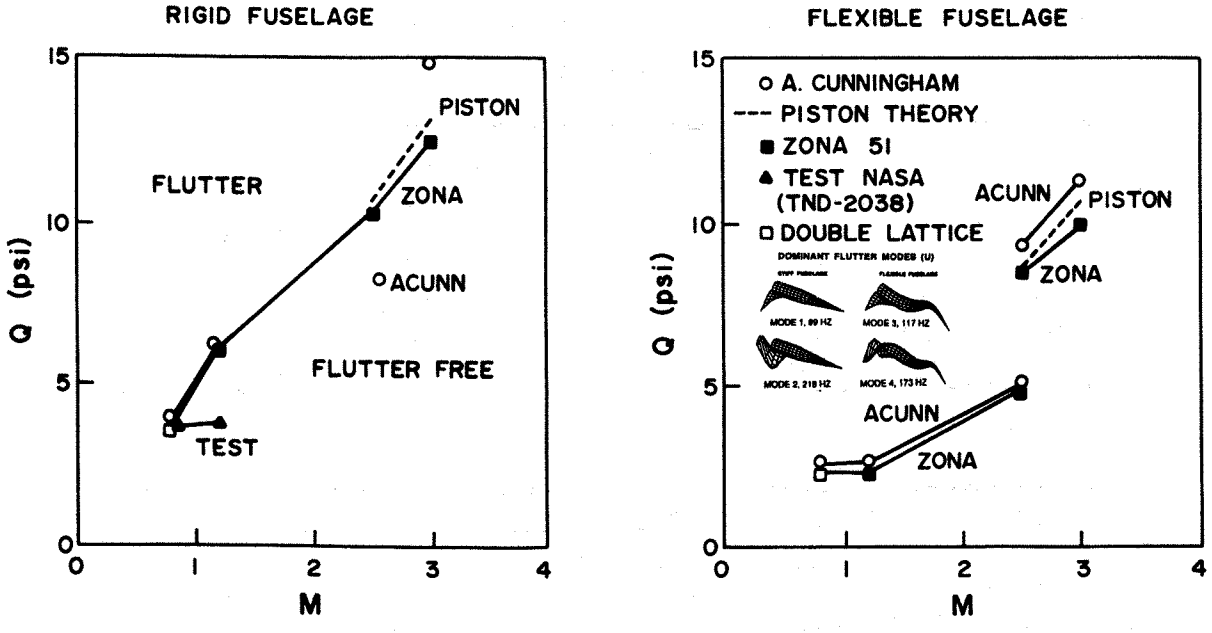

Fig. 24 Flutter Boundaries for NASA Wing-Body Configurations.
a) Rigid Fuselage
b) Flexible Fuselage

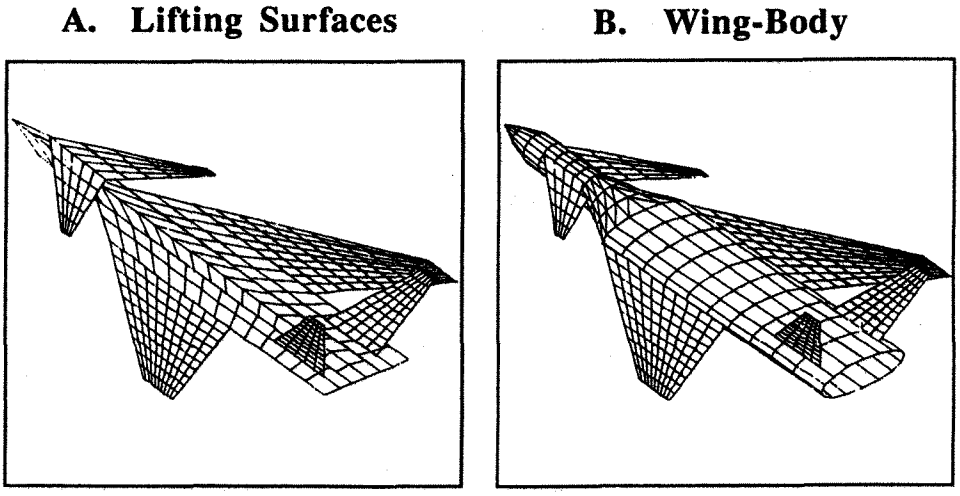

Fig. 25 (a) Model A of LGF: Lifting Surface Model.
(b) Model B of LGF: Wing-Body Model.

TABLE 1. Stability Derivative Comparisons for Models A and B at LGF

(a) M = 1.2

	C_{L_α}		C_{M_α}		$C_{L_\alpha} + C_{L_q}$		$C_{M_\alpha} + C_{L_q}$	
	A	B	A	B	A	B	A	B
Fuselage	.949	.919	-.242	.046	2.417	4.438	-1.462	-4.576
Wing	1.839	1.691	-.894	-.815	1.189	1.235	-.597	-.673
Canard	.715	.630	.600	.506	-.780	-.566	-.663	-.466
Fin	.139	.274	-.192	-.390	.285	-1.083	-.379	1.600
Total	3.640	3.440	-.728	-.651	3.112	4.025	-3.102	-4.126

(b) M = 1.35

	C_{L_α}		C_{M_α}		$C_{L_\alpha} + C_{L_q}$		$C_{M_\alpha} + C_{L_q}$	
	A	B	A	B	A	B	A	B
Fuselage	.948	.966	-.239	-.288	2.201	1.796	-1.432	-1.343
Wing	1.783	1.697	-.838	-.802	.908	.993	-.523	-.584
Canard	.646	.593	.543	.485	-.693	-.574	-.591	-.475
Fin	.121	.123	-.167	-.170	.271	.104	-.359	-.142
Total	3.497	3.383	-.702	-.773	2.687	2.318	-2.905	-2.548

(c) M = 1.50

	C_{L_α}		C_{M_α}		$C_{L_\alpha} + C_{L_q}$		$C_{M_\alpha} + C_{L_q}$	
	A	B	A	B	A	B	A	B
Fuselage	.939	.655	-.236	-.012	1.982	1.503	-1.372	-1.337
Wing	1.745	1.705	-.818	-.828	.547	.604	-.350	-.347
Canard	.593	.560	.501	.460	-.637	-.554	-.547	-.461
Fin	.101	.107	-.140	-.148	.247	.124	-.327	-.170
Total	3.376	3.029	-.694	-.527	2.139	1.668	-2.597	-2.319